5478 *Organometallics* **2009,** *28,* 5478–5488
DOI: 10.1021/om9003785

ORGANOMETALLICS
Article

Phenyl-1*H*-[1,2,3]triazoles as New Cyclometalating Ligands for Iridium(III) Complexes

Beatrice Beyer,[†] Christoph Ulbricht,[‡] Daniel Escudero,[§] Christian Friebe,[†] Andreas Winter,[‡] Leticia González,*[,§] and Ulrich S. Schubert*[,†,‡]

[†]*Laboratory of Organic and Macromolecular Chemistry, Friedrich-Schiller-Universität Jena, Humboldtstrasse 10, 07743 Jena, Germany,* [‡]*Laboratory of Macromolecular Chemistry and Nanoscience, Eindhoven University of Technology, P.O. Box 513, 5600 MB Eindhoven, The Netherlands, and* [§]*Laboratory of Theoretical Chemistry, Friedrich-Schiller-Universität Jena, Helmholtzweg 4, 07743 Jena, Germany*

Received May 11, 2009

We report on the synthesis and characterization of bis-cyclometalated iridium(III) complexes with 4-phenyl-1*H*-[1,2,3]triazole, synthesized via a "click"-chemistry approach, as a new type of cyclometalating ligand. The photophysical and electrochemical properties of these complexes are investigated experimentally as well as theoretically by using density functional theory. The properties of these new complexes are compared to their known 2-phenylpyridinato analogues. The emission of the herein described complexes is clearly influenced by the applied ancillary ligand and can be adjusted over a broad range of frequencies. The results indicate that the phenyl-1*H*-[1,2,3]triazole ligands in general cause a spectral blue shift.

Introduction

Organic light-emitting diodes (OLEDs) have received considerable attention during recent years in the academic world and in industry for display and lighting applications.[1−6] For the fabrication of high-efficiency OLEDs, the development of high-performance materials plays an important role. Iridium(III) complexes show, in contrast to complexes based on other heavy-metal atoms (e.g., Ru^{II}, Rh^{I}, Os^{II}), an intense phosphorescence at room temperature.[7] This emission originates from a triplet metal-to-ligand charge transfer (MLCT) or in some cases from a triplet ligand-centered (LC) state. Due to the strong spin−orbit coupling, the phosphorescent lifetimes are in the microsecond regime. Besides the advantage of obtaining an internal quantum efficiency of theoretically up to 100% in electroluminescent devices,[8] the emission color of iridium(III) complexes can easily be varied from blue to red by adapting the coordinated ligand system. Several strategies have been reported in order to tune the photophysical properties of these complexes and to achieve blue emission, e.g., employing electron-withdrawing substituents in the cyclometalating ligand[9] and using cationic[10] as well as anionic Ir^{III} complexes.[11] In recent years many different ligand systems were investigated in order to obtain phosphors with high quantum yields and color purity. In particular bis- and tris-cyclometalated iridium(III) complexes exhibit a high potential for applications in OLEDs. To form bis-cyclometalated species chloro-bridged dimeric iridium(III) precursors can be reacted with a broad variety of coordination motifs, e.g. bipyridine, picolinate, acetylacetonate, and their derivatives.[12−17] Besides the straightforward synthesis, the utilization of ancillary ligands provides further options to introduce functionalities and to tune the optical and electrical properties. For the understanding of the photophysical behavior of such Ir^{III} complexes, theoretical investigations have proven to be very useful.[11,18]

*Corresponding author. Fax: +49 3641 948302. E-mail: leticia.gonzalez@uni-jena.de. Fax: +49 3641 948202. E-mail: ulrich.schubert@uni-jena.de.

(1) Lowry, M. S.; Bernhard, S. *Chem.—Eur. J.* **2006**, *12*, 7970–7977.
(2) D'Andrade, B. W.; Forrest, S. R. *Adv. Mater.* **2004**, *16*, 1585–1595.
(3) Holder, E.; Langeveld, B. M. W.; Schubert, U. S. *Adv. Mater.* **2005**, *17*, 1109–1121.
(4) Forrest, S. R.; Thompson, M. E. *Chem. Rev.* **2007**, *107*, 923–925.
(5) Müllen, K.; Scherf, U. *Organic Light-Emitting Devices*; Wiley-VCH: Weinheim, Germany, 2006.
(6) Ulbricht, C.; Beyer B.; Friebe C.; Winter, A.; Schubert, U. S. *Adv. Mater.* **2009**, DOI: 10.1002/adma.200803537.
(7) Yersin, H. *Highly Efficient OLEDs with Phosphorescent Materials*; Wiley-VCH: Weinheim, Germany, 2008.
(8) Baldo, M. A.; Lamansky, S.; Burrows, P. E.; Thompson, M. E.; Forrest, S. R. *Appl. Phys. Lett.* **1999**, *75*, 4–6.
(9) Gu, X.; Fei, T.; Zhang, H.; Xu, H.; Yang, B.; Ma, Y.; Liu, X. *J. Phys. Chem. A* **2008**, *112*, 8387–8393.
(10) Zeng, X.; Tavasli, M.; Perepichka, I. F.; Batsanov, A. S.; Bryce, M. R.; Chiang, C.-J.; Rothe, C.; Monkman, A. P. *Chem.—Eur. J.* **2008**, *14*, 933–943.
(11) Di Censo, D.; Fantacci, S.; De Angelis, F.; Klein, C.; Evans, N.; Kalyanasundaram, K.; Bolink, H. J.; Grätzel, M.; Nazeeruddin, M. K. *Inorg. Chem.* **2008**, *47*, 980–989.
(12) Lamansky, S.; Djurovich, P.; Murphy, D.; Abdel-Razzaq, F.; Lee, H.-E.; Adachi, C.; Burrows, P. E.; Forrest, S. R.; Thompson, M. E. *J. Am. Chem. Soc.* **2001**, *123*, 4304–4312.
(13) You, Y. M.; Park, S. Y. *J. Am. Chem. Soc.* **2005**, *127*, 12438–12439.
(14) Kwon, T.-H.; Kim, M. K.; Kwon, J.; Shin, D.-Y.; Park, S.-J.; Lee, C.-L.; Kim, J.-J.; Hong, J. I. *Chem. Mater.* **2007**, *19*, 3673–3680.
(15) Tsuzuki, T.; Shirasawa, N.; Suzuki, T.; Tokito, S. *Adv. Mater.* **2003**, *15*, 1455–1458.
(16) Zhen, H.; Luo, J.; Yang, W.; Chen, Q.; Ying, L.; Jianhua, Z.; Wu, H.; Cao, Y. *J. Mater. Chem.* **2007**, *17*, 2824–2831.
(17) Li, J.; Djurovich, P. I.; Alleyne, B. D.; Yousufuddin, M.; Ho, N. N.; Thomas, J. C.; Peters, J. C.; Bau, R.; Thompson, M. E. *Inorg. Chem.* **2005**, *44*, 1713–1727.
(18) Tamayo, A. B.; Alleyne, B. D.; Djurovich, P. I.; Lamansky, S.; Tsyba, I.; Ho, N. N.; Bau, R.; Thompson, M. E. *J. Am. Chem. Soc.* **2003**, *125*, 7377–7387.

 Published on Web 08/25/2009

In the past decade, the synthesis of 1*H*-[1,2,3]triazoles experienced a great revival in the form of the copper(I)-catalyzed Huisgen cycloaddition. This procedure was introduced independently by the groups of K. B. Sharpless and M. Meldal.[19−21] The addition of a Cu^{I} catalyst leads to the exclusive formation of the 1,4-regioisomer, increases the reaction rate by a factor of 10^7, and enables the performance of the reaction under mild conditions.[22] With this so-called "click" reaction it is possible to introduce different functionalities via the acetylene and the organic azide. Weck and coworkers used the efficient cycloaddition reaction to attach alkyne-functionalized tris-cyclometalated iridium(III) complexes to azide-bearing polymeric backbones, yielding phosphorescent polymers.[23] Performing the "click" reaction with alkyne-functionalized terpyridine moieties at an azide-terminated monolayer Haensch et al. anchored coordination sites to a surface. After the reaction with a dimeric precursor surface-tethered bis-cyclometalated iridium(III) complexes were obtained.[24] Besides the utilization of the "click" reaction as a linking tool [1,2,3]triazoles can be applied as coordination motifs. "Clicked" terpyridine[25,26] and bipyridine[27] analogues were recently introduced and applied in the formation of the respective ruthenium(II) complexes. While 1,2,4-triazoles are established moieties in ancillary ligands applied to synthesize neutral iridium(III) complexes[28−33] and even appear in bpy analogues[34] and cyclometalating[35] systems, the potential of [1,2,3]triazoles as coordination site for iridium(III) species is investigated only marginally. In an early work by Nonoyama et al. 2-aryl-4,5-dimethyl-[1,2,3]-triazoles were used as cyclometalating ligands in the formation of dimeric iridium(III) precursor complexes.[36] A similar dimer with 2-phenyl-2*H*-[1,2,3]triazolo[4,5-*f*]quinoline as cyclometalating ligands was synthesized by Tomkutė-Lukšienė et al. and was further reacted with acetoacetone to yield the respective bis-cyclometalated iridium(III) complex.[37] Orselli et al. applied 2-(1*H*-[1,2,3]triazol-5-yl)pyridine and 2-[4-(aryl)-1*H*-[1,2,3]triazol-5-yl]pyridines as ancillary ligands in the formation of neutral bis-cyclometalated iridium(III) complexes.[38] Phenyl-1*H*-[1,2,3]triazoles with variable substituents in 1- and 4-position, easily accessible by "clicking" the respective azides and acetylenes moieties, have not been investigated regarding potential applications as cyclometalating ligands in the coordination of iridium(III) species, so far.

Here, we report on the synthesis and characterization of new heteroleptic iridium(III) complexes using phenyl-1*H*-[1,2,3]triazoles as cyclometalating ligands. "Click" chemistry was used for the straightforward synthesis of two different types of potential ligand systems. The properties of the new phosphors were analyzed and compared to classical complexes based on 2-phenylpyridine (Hppy). In addition, a DFT and time-dependent DFT (TD-DFT) study of the ground and excited states of selected Ir^{III} complexes has been performed in order to interpret the experimental photophysical data. This study provides valuable information regarding the excited states involved in the absorption and emission processes.

Results and Discussion

Synthesis and Characterization. The synthesis of the new cyclometalating ligands was carried out in a highly efficient one-pot consecutive procedure. Following literature descriptions, the respective acetylene derivative was reacted with the organic azide, formed *in situ* from the corresponding bromo compound.[39,40] It is noteworthy that no further copper(I) catalyst had to be added after the formation of the arylazide in order to perform the "click" reaction. The so-called "click" rules, as specified by Sharpless,[20] were completely fulfilled. After reacting the organic azides and acetylene compounds in an environmentally friendly solvent mixture (i.e., ethanol/water, 7:3 ratio) at room temperature, the potential ligands 1-decyl-4-phenyl-1*H*-[1,2,3]triazole (**H-a**) and 4-decyl-1-phenyl-1*H*-[1,2,3]triazole (**H-b**) could be obtained in high yields by simple purification procedures (Scheme 1). The formation of only one triazole regioisomer was verified by ^{1}H NMR spectroscopy. The signal originating from the *ortho*-protons of the phenyl ring (asterisk in Figure 1) is significantly high-field shifted for **H-a** (7.84 ppm) and **H-b** (7.75 ppm) in comparison to 2-phenylpyridine (Hppy, 8.04 ppm). This can be explained by the higher electron density in the phenyl ring due to mesomerism of the lone electron pairs of the triazole nitrogen atoms to the attached phenyl ring. Furthermore, the ligands were characterized by ^{13}C NMR and UV−vis absorption spectroscopy as well as MALDI-TOF mass spectrometry and elemental analysis.

(19) Tornøe, C. W.; Christensen, C.; Meldal, M. *J. Org. Chem.* **2002**, *67*, 3057–3064.
(20) Kolb, H. C.; Finn, M. G.; Sharpless, K. B. *Angew. Chem., Int. Ed.* **2001**, *40*, 2004–2021.
(21) Rostovtsev, V. V.; Green, L. G.; Fokin, V. V.; Sharpless, K. B. *Angew. Chem., Int. Ed.* **2002**, *41*, 2596–2599.
(22) Bock, V. D.; Hiemstra, H.; Maarseveen, J. H. *Eur. J. Org. Chem.* **2006**, *1*, 51–68.
(23) Wang, X.-Y.; Kimyonok, A.; Weck, M. *Chem. Commun.* **2006**, 3933–3935.
(24) Haensch, C.; Chiper, M.; Ulbricht, C.; Winter, A.; Hoeppener, S.; Schubert, U. S. *Langmuir* **2008**, *24*, 12981–12985.
(25) Li, Y. J.; Huffman, J. C.; Flood, A. H. *Chem. Commun.* **2007**, 2692–2694.
(26) Schulze, B.; Friebe, C.; Hager, M. D.; Winter, A.; Hoogenboom, R.; Görls, H.; Schubert, U. S. *Dalton* **2009**, 787–794.
(27) Happ, B.; Friebe, C.; Winter, A.; Hager, M. D.; Hoogenboom, R.; Schubert, U. S. *Chem. Asian. J.* **2009**, *4*, 154–163.
(28) Yang, C.-H.; Li, S.-W.; Chi, Y.; Cheng, Y.-M.; Yeh, Y.-S.; Chou, P.-T.; Lee, G.-H.; Wang, C.-H.; Shu, C.-F. *Inorg. Chem.* **2005**, *44*, 7770–7780.
(29) Liang, B.; Jiang, C.; Chen, Z.; Zhang, X.; Shi, H.; Cao, Y. *J. Mater. Chem.* **2006**, *16*, 1281–1286.
(30) Takizawa, S.-y.; Nishida, J.-i.; Tsuzuki, T.; Tokito, S.; Yamashita, Y. *Inorg. Chem.* **2007**, *46*, 4308–4319.
(31) Liang, B.; Wang, L.; Xu, Y.; Shi, H.; Cao, Y. *Adv. Funct. Mater.* **2007**, *17*, 3580–3589.
(32) Chang, C.-F.; Cheng, Y.-M.; Chi, Y.; Chiu, Y.-C.; Lin, C.-C.; Lee, G.-H.; Chou, P.-T.; Chen, C.-C.; Chang, C.-H.; Wu, C.-C. *Angew. Chem., Int. Ed.* **2008**, *47*, 4542–4545.
(33) Song, Y.-H.; Chiu, Y.-C.; Chi, Y.; Cheng, Y.-M.; Lai, C.-H.; Chou, P.-T.; Wong, K.-T.; Tsai, M.-H.; Wu, C.-C. *Chem.—Eur. J.* **2008**, *14*, 5423–5434.
(34) van Diemen, J. H.; Haasnoot, J. G.; Hage, R.; Müller, E.; Reedijk, J. *Inorg. Chim. Acta* **1991**, *181*, 245–251.
(35) Lo, S.-C.; Shipley, C. P.; Bera, R. N.; Harding, R. E.; Cowley, A. R.; Burn, P. L.; Samuel, I. D. W. *Chem. Mater.* **2006**, *18*, 5119–5129.
(36) Nonoyama, M.; Hayata, C. *Transition Met. Chem.* **1978**, *3*, 366–369.
(37) Tomkutė-Lukšienė, D.; Malinauskas, T.; Stanišauskaitė, A.; Getautis, V.; Kazlauskas, K.; Vitta, P.; Žukauskas, A.; Juršėnas, S. *J. Photochem. Photobiol. A: Chem.* **2008**, *198*, 106–110.
(38) Orselli, E.; Albuquerque, R. Q.; Fransen, P. M.; Fröhlich, R.; Janssen, H. M.; De Cola, L. *J. Mater. Chem.* **2008**, *18*, 4579–4590.
(39) Ju, Y.; Kumar, D.; Varma, R. S. *J. Org. Chem.* **2006**, *71*, 6697–6700.
(40) Anderson, J.; Madsen, U.; Björkling, F.; Liang, X. *Synlett* **2005**, 2209–2213.

Scheme 1. Schematic Representation of the Synthesis of the Potential Ligands H-a and H-b

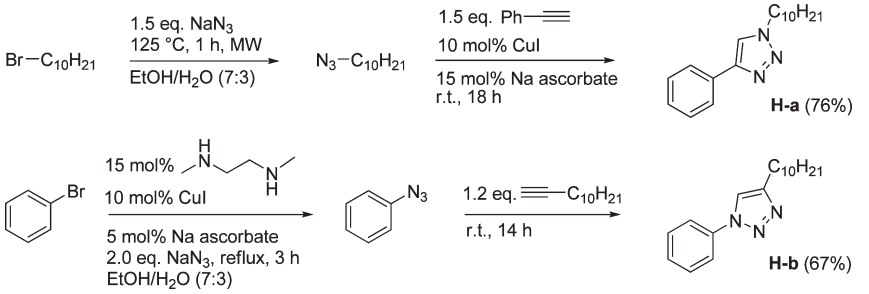

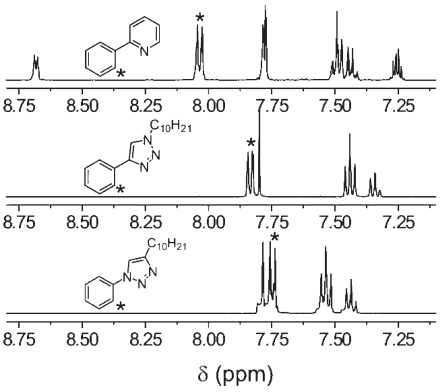

Figure 1. ^{1}H NMR spectra (aromatic region) of Hppy (top), **H-a** (middle), and **H-b** (bottom). For all spectra: 400 MHz, room temperature, CD_2Cl_2.

Although the "click" reaction offers many advantages to easily engineer heterocycles, it has one inherent drawback. The handling of organic azides is connected with certain safety considerations.[41] Therefore, it was not advisible to synthesize 4-phenyl-[1,2,3]triazoles with short alkyl chains. For comparison, the same alkyl chain length was used for ligands **H-a** and **H-b**. However, the presence of the required alkyl chains dramatically reduced the probability of obtaining single crystals suitable for X-ray analysis.

The synthesized phenyl-triazole derivatives **H-a** and **H-b** as well as the commercially available 2-phenylpyridine were reacted with $IrCl_3 \times 3H_2O$ to form the respective dimeric chloro-bridged iridium(III) precursor complexes following literature procedures (Scheme 2).[42] The isolated yields of the new dimeric precursors **A** and **B** were good (76% and 53%, respectively), but lower than that of [(Ir(ppy)$_2$-μ-Cl)$_2$] (**C**, 90% yield). This might be attributed to the circumstance that column chromatography was necessary as an additional purification step (**A**, **B** vs **C**) and the slightly lower ability of the phenyl-1*H*-[1,2,3]trizoles to form stable carbanions for the cyclometalation due to the increased electron density in the C$^{2'}$-position, as already observed by ^{1}H NMR spectroscopy. Despite thorough purification, the NMR spectra recorded from precursors **A** and **B** appeared rather undefined. However, elemental analyses showed good compositional consistency with the expected molecular formula of a dimeric precursor complex. Since the desired bis-cyclometalated Ir^{III} complexes could be synthesized in the following with precursor **A**, it is assumed that not only dimeric complexes with D_2-symmetry, as predicted for the ppy-based precursor,[43] were formed. In a precursor with C_{2h}-symmetry the coordinating nitrogen atoms would still be in *trans*-position to each other, and thus, the ligands in the resulting heteroleptic complexes would have the same configuration as originating from a D_2-precursor.

The general synthetic routes toward different types of bis-cyclometalated complexes are summarized in Scheme 3. Heteroleptic complexes deriving from precursor **A** could be isolated in similar or even higher yields compared to the analogous ppy-based complexes. The charged iridium(III) complexes were synthesized applying an excess (5 to 9 equiv) of the respective bidentate ligand, i.e., 2,2′-bipyridine (bpy) or 2-(1-decyl-1*H*-[1,2,3]triazol-4-yl)pyridine (trpy). After 14 h refluxing in a solvent mixture of CH_2Cl_2/CH_3OH (4:5), an anion exchange with NH_4PF_6 was performed. The neutral complexes were obtained from the reaction with either acetylacetone (Hacac, 10 equiv) or picolinic acid (Hpic, 5 equiv) in the presence of equimolar amounts of Na_2CO_3 by refluxing for 14 h in C_2H_5OH and CH_2Cl_2, respectively.

Starting from precursor **B**, the expected heteroleptic complexes could not be isolated, with exception of complex [Ir(**b**)$_2$(acac)]. Due to the poor yield of approximately 5% a full characterization of this complex could not be carried out. In all other cases, either many byproducts were formed, in particular for the charged systems (i.e., bpy and trpy) or the attempts to cleave the chloro bridge to form neutral complexes failed. The instability of the crude products on the column material prevented any purification by column chromatography. In addition, the release of the cyclometalating ligand (i.e., **H-b**) during the synthetic attempts with precursor **B** could be observed as well. It is supposed that the thermodynamic stability of complexes originating from **H-b** is remarkably lower than for complexes synthesized from **H-a**. Thus, the position of the cyclometalating phenyl ring seems to be important for the σ-donor and π-acceptor strength of the new ligands. As already concluded from the ^{1}H NMR spectra of these two types of ligands, **H-b** features a higher electron density than **H-a** in the phenyl ring. Apparently, the π-back-donation from the Ir^{III} center to the ligand **b** is also less pronounced.

Electro-optical Properties. The experimental UV−vis absorption spectra of both 2-phenylpyridine- (Ir(ppy)$_2$L^X) and phenyl-1*H*-[1,2,3]triazole-containing complexes (Ir(a)$_2$-L^X), are depicted in Figure 2. The corresponding photoluminescence (PL) spectra are shown in Figure 3. The

(41) Bräse, S.; Gil, C.; Knepper, K.; Zimmermann, V. *Angew. Chem., Int. Ed.* **2005**, *44*, 5188–5240.
(42) Winter, A.; Ulbricht, C.; Holder, E.; Risch, N.; Schubert, U. S. *Aust. J. Chem.* **2006**, *59*, 773–782.
(43) Sprouse, S.; King, K. A.; Spellane, P. J.; Watts, R. J. *J. Am. Chem. Soc.* **1984**, *106*, 6647–6653.

Scheme 2. Schematic Representation of the Synthesis of the Dimeric Iridium(III) Precursor Complexes $[Ir(C^{\wedge}N)_2\text{-}\mu\text{-}Cl]_2$

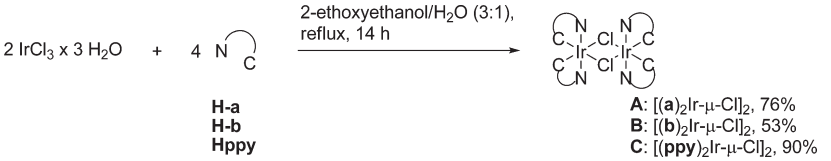

Scheme 3. Schematic Representation of the Synthesis of Heteroleptic Iridium(III) Complexes[a]

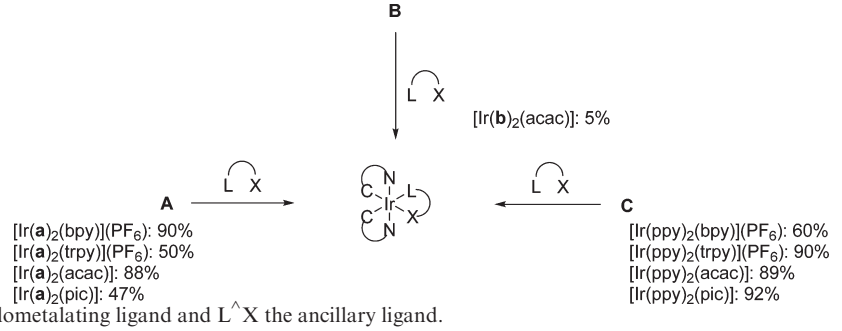

[a] $C^{\wedge}N$ represents the cyclometalating ligand and $L^{\wedge}X$ the ancillary ligand.

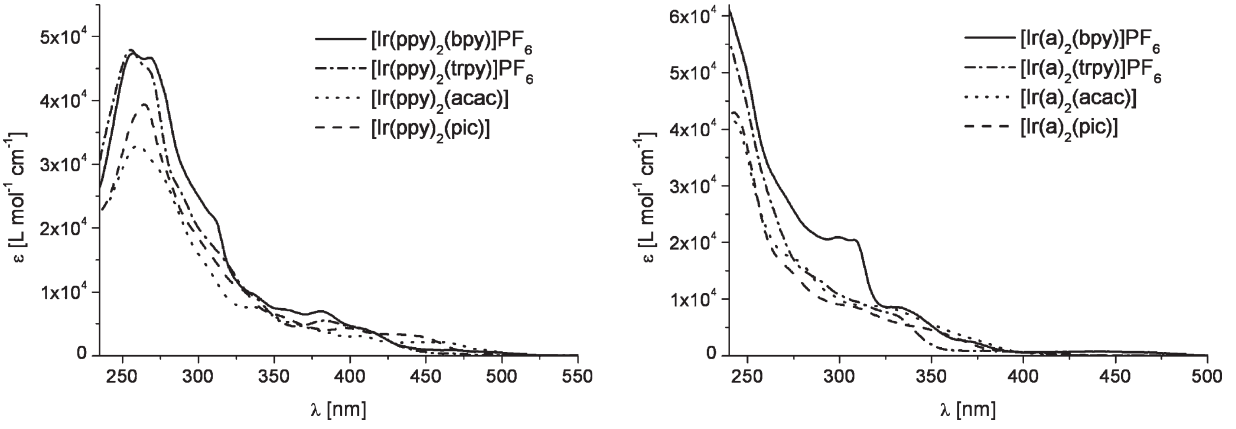

Figure 2. Experimental UV−vis absorption spectra of the Ir^{III} complexes containing ppy (left) and **a** (right) as cyclometalating ligand. For all spectra: 10^{-6} M in CH_2Cl_2, room temperature.

photophysical and electrochemical characteristics of the complexes are summarized in Tables 1 and 2.

It is noteworthy that in the case of the complexes based on 2-phenylpyridine (i.e., $[Ir(ppy)_2(acac)]$, $[Ir(ppy)_2(bpy)](PF_6)$, and $[Ir(ppy)_2(pic)]$) the observed data (Table 1) are in accordance with the values reported in the literature.[12,44,46] Furthermore the experimental spectra reveal the expected absorption blue-shifts for the [1,2,3]triazole-derived complexes in comparison to their 2-phenylpyridine counterparts, while the shape of the absorption bands exhibits a high resemblance.

In order to gain a more detailed insight into the photophysical properties of the (phenyl-1*H*-[1,2,3]triazole)-based Ir^{III} complexes, theoretical Δ-DFT and TD-DFT (B3LYP/TZVP) calculations have been performed for $[Ir(\mathbf{a})_2(bpy)]^+$, $[Ir(\mathbf{a})_2(acac)]$, and $[Ir(\mathbf{a})_2(pic)]$. Figure 4 shows the obtained Kohn−Sham frontier orbitals and the energy level schemes of the three complexes.

In the neutral complexes the highest occupied molecular orbitals (HOMOs) are the t_{2g}-orbital set of the central Ir^{III} ion. In the case of $[Ir(\mathbf{a})_2(bpy)]^+$, however, a π-orbital of the cyclometalating ligand is intercalated within the occupied 5d-orbitals. For all complexes the HOMO corresponds to the $5d_{xy}$-orbital, while the LUMO is a π^*-orbital. Interestingly, this antibonding orbital is located on the ancillary ligand in the case of $[Ir(\mathbf{a})_2(bpy)]^+$ and $[Ir(\mathbf{a})_2(pic)]$ but on the cyclometalating ligand in the case of $[Ir(\mathbf{a})_2(acac)]$. The following unoccupied orbitals are mostly of π^*-antibonding character (not specified in Figure 4). The e_g-orbitals of Ir^{III} are, as seen in Figure 4, strongly destabilized in these complexes. This is a common feature for cyclometalated Ir^{III} complexes, since the strong ligand field effect of the phenyl anion ligand increases the gap between the t_{2g}- and e_g-orbitals. Thus, $5d_{z^2}$ and $5d_{x^2}-y^2$ correspond to LUMO+11 and LUMO+13 in $[Ir(\mathbf{a})_2(bpy)]^+$, respectively, while in $[Ir(\mathbf{a})_2(pic)]$ and $[Ir(\mathbf{a})_2(acac)]$ they relate to LUMO+10 and LUMO+12. The energetic gaps between the HOMO and LUMO levels are also noted in Figure 4. As stated in the introduction, a blue-shifted emission in Ir^{III} systems can be achieved by properly choosing the substituents on the

(44) Lo, K. K.-W.; Chan, J. S.-W.; Lui, L.-H.; Chung, C.-K. *Organometallics* **2004**, *23*, 3108–3116.
(45) Nastasi, F.; Puntoriero, F.; Campagna, S.; Schergna, S.; Maggini, M.; Cardinali, F.; Delavaux-Nicot, B.; Nierengarten, J.-F. *Chem. Commun.* **2007**, 3556–3558.
(46) Gupta, D.; Katiyar, M.; Deepak; Hazra, T.; Verma, A.; Manoharan, S. S.; Biswas, A. *Opt. Mater.* **2006**, *28*, 1355–1361.

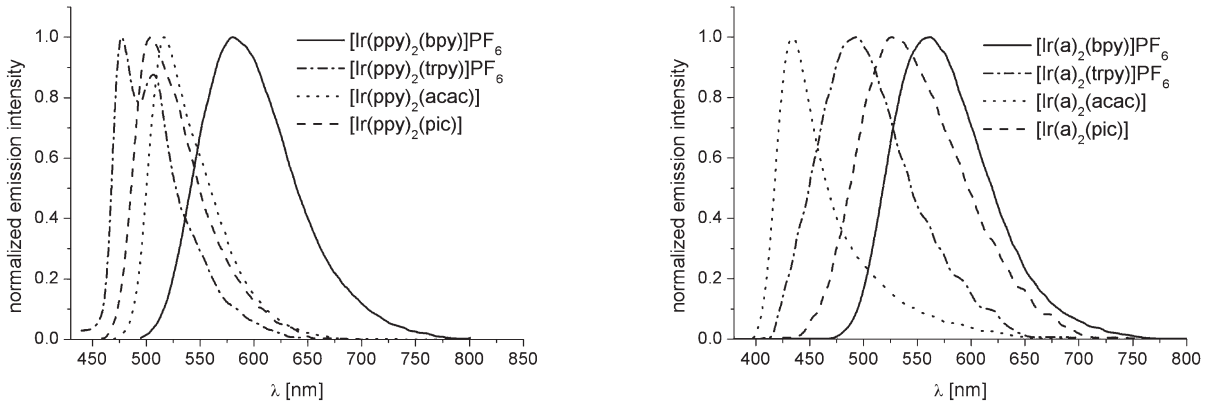

Figure 3. Photoluminescence spectra of the Ir^{III} complexes containing ppy (left) and **a** (right) as cyclometalating ligand. For all spectra: 10^{-7} M in degassed CH_2Cl_2, room temperature, excitation at longest absorption wavelength.

Table 1. Selected Photophysical Properties of the Investigated Ir^{III} Complexes

complex	λ_{abs} [nm] (log ε)[a]	λ_{PL} [nm][b]	E_{0-0} [nm][c]	Φ_{PL}[b,d]
$[Ir(a)_2(bpy)](PF_6)$	240 (4.79), 299 (4.32), 330 (3.93), 441 (2.88), 470 (2.74)	560	474	0.45
$[Ir(a)_2(trpy)](PF_6)$	240 (4.74), 329 (3.87), 378 (2.92)	495	415	0.29
$[Ir(a)_2(acac)]$	241 (4.62), 276 (4.23), 318 (3.95)	435	400	0.02
$[Ir(a)_2(pic)]$	243 (4.63), 303 (3.95), 347 (3.68), 399 (2.82)	527	440	0.11
$[Ir(ppy)_2(bpy)](PF_6)$	257 (4.68), 269 (4.67), 381 (3.85), 466 (2.94), 492 (2.74)	580	498	0.29
$[Ir(ppy)_2(trpy)](PF_6)$	256 (4.68), 266 (4.65), 382 (3.74), 408 (3.63)	477, 507	451	0.21
$[Ir(ppy)_2(acac)]$	260 (4.52), 337 (3.88), 405 (3.49), 456 (3.32), 489 (2.94)	517	481	0.53
$[Ir(ppy)_2(pic)]$	264 (4.60), 398 (3.64), 429 (3.53), 477 (2.83)	505	467	0.29

[a] Measured in CH_2Cl_2, 10^{-6} M, room temperature. [b] Measured in degassed CH_2Cl_2, 10^{-7} M, room temperature. [c] The 0−0 vibration gap is estimated by the intersection of absorption and emission spectra. [d] Absolute quantum yields.

cyclometalating ligands as well as on the ancillary ligand, which stabilizes the HOMO and/or destabilizes the LUMO and, thus, increases the HOMO−LUMO energy gap.[13,47] For the complexes studied herein we have obtained decreasing theoretical energy gaps of 4.31, 3.68, and 3.21 eV for $[Ir(\mathbf{a})_2(acac)]$, $[Ir(\mathbf{a})_2(pic)]$, and $[Ir(\mathbf{a})_2(bpy)]^+$, respectively. This trend has been confirmed by electrochemical data derived from cyclic voltammetry investigations (Table 2). There, the HOMO energy levels, which were calculated from the oxidation potentials (assigned to a reversible Ir^{III}/Ir^{IV} oxidation), show good agreement with the calculated values. Since, except for the case of the bpy systems, the reduction potentials appear out of the accessible range of the cyclic voltammetry measurements, the LUMO energies were determined by using the optical band gaps estimated from the absorption spectra. In comparison to the experimentally derived data, values obtained by the theoretical calculations show particularly an overestimation regarding the LUMO levels and, therefore, also for the theoretical band gaps E_g. However the relative change within the complex series is consistent for both the LUMO energies and the HOMO−LUMO energy gaps ($E_g^{acac} > E_g^{pic} > E_g^{bpy}$), see Table 2.

Previous theoretical studies have dealt with the well-known $[Ir(ppy)_2(L\hat{}X)]$-type derivatives.[49,50] For instance, for $[Ir(ppy)_2(acac)]$ an energetic gap of 3.46 eV was obtained also using the B3LYP functional. On the basis of these data we can evaluate the influence of the cyclometalating ligand (i.e., **a** vs ppy) on the HOMO−LUMO gap. Apparently, ligand **a** increases the energy gap (4.31 eV) as compared to the ppy ligand-based complex (3.46 eV).[50] This difference stems from both the stabilization of the HOMO and the destabilization of the LUMO, which can both be caused by the increased π-acceptor ability of the [1,2,3]triazole moiety. The enhanced possibility to receive electron density in the π^*-orbitals of the ligand-centered π-system via back-bonding stabilizes the occupied t_{2g}-orbitals of the iridium. On the other hand it also destabilizes the unoccupied π^*-orbitals of the ligands including the LUMO level.

By analyzing the effect of the ancillary ligand (i.e., bpy, acac, pic) on the energetic ordering of the frontier orbitals, several points arise. First, a larger band gap is observed for the neutral compounds in comparison to the cationic $[Ir(\mathbf{a})_2(bpy)]^+$ complex. It has been reported previously that by using cationic Ir^{III} complexes the HOMO energies are stabilized, and, thus, larger energy gaps can be achieved.[11,50] Indeed, the HOMO orbital is stabilized in the cationic compound studied here, namely, $[Ir(\mathbf{a})_2(bpy)]^+$, in comparison to the neutral complexes. However, the LUMO is more stabilized to a major extent than the HOMO, and as a consequence, the HOMO−LUMO energy gap is reduced. Second, a comparison between the neutral compounds (i.e., $[Ir(\mathbf{a})_2(acac)]$ and $[Ir(\mathbf{a})_2(pic)]$) shows that the major differences between them originate from the LUMO energies rather than the HOMO energies. As stated above, both LUMOs show π^*-character, but are located on the cyclometalating and on the ancillary ligand, respectively. In $[Ir(\mathbf{a})_2(pic)]$ the LUMO located on the ancillary ligand (π^*_{anc}) is stabilized with respect to the π^*_{anc}-orbital in $[Ir(\mathbf{a})_2(acac)]$, which lies higher in energy than the π^*-orbital of the cyclometalating ligands. This fact can be attributed to the higher conjugation of

(47) Sajoto, T.; Djurovich, P. I.; Tamayo, A.; Yousufuddin, M.; Bau, R.; Thompson, M. E.; Holmes, R. J.; Forrest, S. R. *Inorg. Chem.* **2005**, *44*, 7992–8003.
(48) Egbe, D. A. M.; Bader, C.; Nowotny, J.; Günther, W.; Klemm, E. *Macromolecules* **2003**, *36*, 5459–5469.
(49) Hay, P. J. *J. Phys. Chem. A*. **2002**, *106*, 1634–1641.
(50) Liu, T.; Xia, B.-H.; Zhou, X.; Zheng, Q.-C.; Pan, Q.-J.; Zhang, H.-X. *Theor. Chem. Acc.* **2008**, *121*, 155–164.

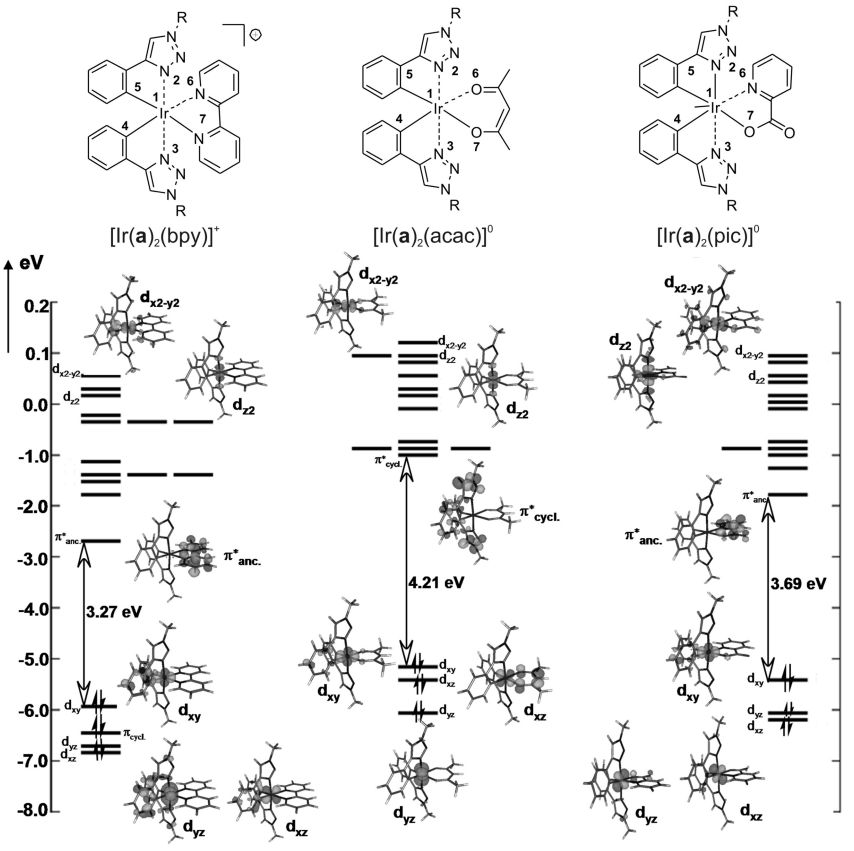

Figure 4. (Top) Schematic representation of the heteroleptic bis-cyclometalated Ir^{III} complexes investigated theoretically herein (R = CH_3, the atom labeling denotes the main geometrical parameters of the gas phase optimized complexes as summarized in Table 5). (Bottom) Energy level schemes for the Kohn−Sham orbitals of the Ir^{III} complexes, including the most relevant Kohn−Sham orbitals and the HOMO−LUMO gaps calculated with B3LYP/TZVP.

Table 2. Electrochemical Data of the Synthesized Ir^{III} Complexes

complex	$E_{1/2,ox}$ [V][a]	E_g^{opt} [eV][b]	E_g^{theo} [eV]	E^{HOMO} [eV][c]	E^{LUMO} [eV][d]
[Ir(**a**)$_2$(bpy)](PF$_6$)	1.23	2.49	3.21	−5.63 (−6.22)[e]	−3.14 (−3.01)[e]
[Ir(**a**)$_2$(trpy)](PF$_6$)	1.20	2.88		−5.59	−2.71
[Ir(**a**)$_2$(acac)]	0.71	3.15	4.31	−5.11 (−5.25)[e]	−1.96 (−0.94)[e]
[Ir(**a**)$_2$(pic)]	0.90	2.82	3.68	−5.29 (−5.54)[e]	−2.47 (−1.86)[e]
[Ir(ppy)$_2$(bpy)](PF$_6$)	1.27	2.37		−5.68	−3.31
[Ir(ppy)$_2$(trpy)](PF$_6$)	1.23	2.76		−5.66	−2.90
[Ir(ppy)$_2$(acac)]	0.76	2.41		−5.18	−2.77
[Ir(ppy)$_2$(pic)]	0.94	2.46		−5.32	−2.86

[a] Measurements were performed in CH_2Cl_2 containing 0.1 M $TBAPF_6$. The potentials are given vs standard hydrogen electrode (SHE). [b] Estimated from the UV−vis spectra at 10% absorption on the longer wavelength side. [c] E^{HOMO} calculated from $E_{1/2,ox}$. [d] Determined from E_g^{opt} and E^{HOMO}.[48] [e] Values obtained at the B3LYP/TZVP level of theory in parentheses.

the π*-orbital in case of the aromatic picolinate ligand. As a consequence, a smaller band gap is obtained for [Ir(**a**)$_2$(pic)].

A comparison of the calculated and experimental absorption spectra for the complexes [Ir(**a**)$_2$(bpy)]$^+$, [Ir(**a**)$_2$(acac)], and [Ir(**a**)$_2$(pic)] is presented in Figure 5. In Table 3 the main electronic singlet−singlet vertical excitations, their oscillator strengths, and their corresponding assignments are summarized. The agreement between the calculated and experimental values is good, notwithstanding that TD-DFT tends to overestimate the charge-transfer (CT) states.[51] On the other hand it is well established that hybrid functionals, such as B3LYP, are less affected by this problem.[52] The experimental spectra show weak absorption bands from 350 to 425 nm (up to 500 nm for the charged bpy complex) with extinction coefficients (ε) in the range 1000 to 5000 $L \cdot mol^{-1} \cdot cm^{-1}$. These bands can be assigned to singlet metal-to-ligand charge-transfer (MLCT) transitions from metal-centered d-orbitals to π*-orbitals localized on either the ancillary or the cyclometalating ligand. The presence of ligand-centered (LC) transitions leads to strong absorption transitions (10 000 to 60 000 $L \cdot mol^{-1} \cdot cm^{-1}$) in the short-wavelength region below 300 nm. The involved molecular orbitals of these transitions are localized either on one ligand (ancillary or cyclometalating) or between different ones.

As shown in Figure 2, no absorption is found above 500 nm. The long tail between 360 and 500 nm, in particular for [Ir(**a**)$_2$(pic)], where singlet−singlet excitations are dark or do not exist, should be then attributed to singlet−triplet excitations (see Table 4). Note that within the computational approach used herein, singlet−triplet excitation energies have no intensity because spin−orbit coupling is neglected in the TD-DFT calculations.

From Table 3 we can conclude that all compounds show common features in their UV−vis absorption spectra. The low-energy range up to 4.50 eV (273 nm) is characterized by MLCT transitions between an orbital of the t_{2g}-set and a π*-antibonding orbital of either the cyclometalating or ancillary

(51) Dreuw, A.; Head-Gordon, M. *Chem. Rev.* **2005**, *105*, 4009–4037.

(52) Dreuw, A.; Weisman, J. L.; Head-Gordon, M. *J. Chem. Phys.* **2003**, *119*, 2943–2946.

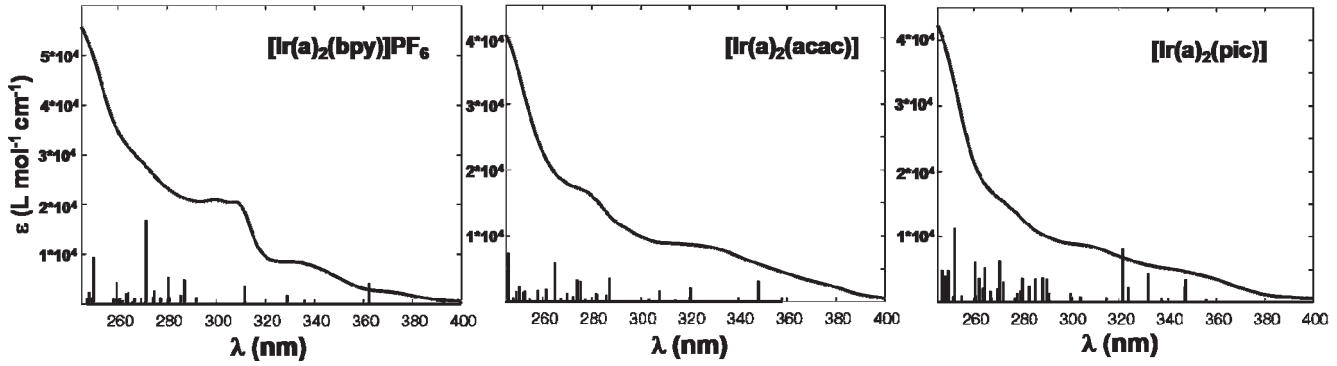

Figure 5. Experimental spectra of Ir^{III} complexes with **a** as cyclometalating ligand (solid line) and TD-DFT (B3LYP/TZVP in CH_2Cl_2) vertical excitations. The oscillator strengths of the vertical excitations have been scaled to the experimental spectra.

ligand. Only for $[Ir(\mathbf{a})_2(bpy)]^+$ is a LC transition, namely, a transition from a π-orbital localized on the cyclometalating ligand (π_{cycl}) to a π^*-orbital localized on the ancillary ligand (π^*_{anc}), found at low energies (see S_2 in Table 3). In particular, for this compound a shoulder of the peak that dominates the UV−vis spectrum can be observed around 300 nm; this peak can be attributed presumably to S_{11} and S_{17}, but is underestimated in terms of oscillator strength. Beyond 4.50 eV, the shape of the spectra of $[Ir(\mathbf{a})_2(bpy)]^+$ is dominated by both LC and MLCT transitions, but mainly by LC transitions in the case of $[Ir(\mathbf{a})_2(acac)]$ and $[Ir(\mathbf{a})_2(pic)]$. Additionally, for $[Ir(\mathbf{a})_2(pic)]$ a metal-centered (MC) transition that corresponds to S_{38} is found.

In the following we turn our attention to the nature of the excited states involved in the emission process, for which both theoretical calculations and experimental photoluminescence measurements were carried out. The PL spectra of all discussed complexes have been depicted in Figure 3. One can clearly see the change of character of the lowest excited state from a ^{3}LC dominated one in the case of $[Ir(ppy)_2(trpy)](PF_6)$—identifiable through a blue-shifted, narrow, and structured band—to a more ^{3}MLCT dominated state for the 2,2′-bipyridine-substituted complex (i.e., red-shifted, broad, and unstructured band). In contrast, the $[Ir(\mathbf{a})_2(L^{\wedge}X)](PF_6)_n$-type complexes (Figure 3, right) feature only emission bands without any structuring, suggesting a ^{3}MLCT character of the emission transitions. This assumption is supported by the obtained calculation results collected in Table 4. It might be caused by the higher HOMO−LUMO energy gaps that are present in the 4-phenyl-1*H*-[1,2,3]triazole moiety compared to the 2-phenylpyridine unit, which lead to a decreased possibility of interaction between the LC transitions and the lower energy MLCT states. Consequently this fact would cause a decreased contribution of LC states to the photoluminescence process in the case of the [1,2,3]triazole-type complexes. The related photoluminescence quantum yields differ significantly (Table 1). They range from nearly no emission in the case of $[Ir(\mathbf{a})_2(acac)]$ ($\Phi_{PL} = 0.02$) to notable values, as for its bpy-match $[Ir(\mathbf{a})_2(bpy)](PF_6)$ ($\Phi_{PL} = 0.45$). Further investigations of the photoluminescence properties, such as PL lifetime measurements, are currently ongoing. In addition, the incorporation of the new bis-cyclometalated Ir^{III} complexes into OLED devices in order to gain more insight into the electro-optical behavior of the emitters and to study the derived device characteristics represents future targets.

For excited Ir^{III} complexes it is well known that the triplet excited states are populated rapidly via efficient intersystem crossing (ISC) between the singlet and triplet photoexcited states (due to the strong spin−orbit coupling induced by the Ir^{III} center). Afterward, internal conversion (IC) and vibrational relaxation (i.e., solvent deactivation) to the lowest triplet excited state (T_1) follow. The theoretical emission energies cannot be directly derived from the calculation of the singlet−triplet excitation transitions. For a given couple of electronic states, the emission intensities are determined by the vibrational wave function overlaps (the Franck−Condon factors) between the lowest vibrational level of the excited state and various vibrational levels of the electronic ground state. Recently, simulations of emission spectra have been achieved for large organic molecules[53] and organometallic complexes.[54]

Here, we restrict ourselves to calculate the emission spectral maxima for $[Ir(\mathbf{a})_2(bpy)]^+$, $[Ir(\mathbf{a})_2(acac)]$, and $[Ir(\mathbf{a})_2(pic)]$; see Table 4. A two-step approach is followed. As a first step, the five lowest lying singlet−triplet excitations were obtained at the TD-B3LYP/TZVP level of theory in the presence of solvent (CH_2Cl_2). Interestingly, in all cases the emissive state (T_1) is of MLCT character. The following triplet excited states are also mainly of ^{3}MLCT character, with the exception of T_3 in $[Ir(\mathbf{a})_2(bpy)]^+$, for which a ^{3}LC state is found. The comparison of the so-obtained excitation energies for T_1 in $[Ir(\mathbf{a})_2(bpy)]^+$ (505 nm), $[Ir(\mathbf{a})_2(acac)]$ (413 nm), and $[Ir(\mathbf{a})_2(pic)]$ (422 nm) with the experimental photoluminescence maxima (560, 435, and 527 nm, respectively, from Table 1) shows a hypsochromic shift for the theoretical values, in particular for the picolinate derivative. Since these complexes possess excited state lifetimes in the microsecond regime, allowing for relaxation to the lowest triplet excited state, and these TD-DFT excitations are vertical transitions from the electronic ground state S_0, blue-shifted peaks are inherent. Therefore, as a second step, triplet state optimizations have been carried out to yield adiabatic emission energies. The T_1 minima of the three compounds are ^{3}MLCT states, with one electron of the HOMO ($5d_{xy}$) promoted to a π^*-orbital. As stated in the computational details, the main geometrical differences with respect to S_0 refer to the shortening of some of the Ir−C$^{\wedge}$N bond distances in the T_1 minima, which has been already discussed for related iridium(III) complexes.[55] As

(53) Santoro, F.; Improta, R.; Lami, A.; Bloino, J.; Barone, V. *J. Chem. Phys.* **2007**, *126*, 084509/1–084509/13.
(54) De Angelis, F.; Santoro, F.; Nazeeruddin, M. K.; Barone, V. *J. Phys. Chem. B* **2008**, *112*, 13181–13183.
(55) De Angelis, F.; Fantacci, S.; Evans, N.; Klein, C.; Zakeeruddin, S. M.; Moser, J-.E.; Kalyanasundaram, K.; Bolink, H. J.; Grätzel, M.; Nazeeruddin, M. K. *Inorg. Chem.* **2007**, *46*, 5989–6001.

Table 3. Main Theoretical Electronic Transitions Energies (ΔE), with Corresponding Oscillator Strengths (f) and Assignment for Cyclometalated Complexes [Ir(a)$_2$(L^X)]

state	ΔE [eV (nm)]	f	assignment	state	ΔE [eV (nm)]	f	assignment
			[Ir(a)$_2$(bpy)]$^+$				
S_1	2.48(500)	0.000	$d_{xy}\rightarrow\pi^*_{anc}$ (70%) MLCT	S_{23}	4.51(275)	0.042	$\pi_{cycl}\rightarrow\pi^*_{cycl}$ (59%) LC
S_2	3.16(393)	0.017	$\pi_{cycl}\rightarrow\pi^*_{anc}$ (70%) LC	S_{25}	4.57(271)	0.262	$d_{xz}\rightarrow\pi^*_{anc}$ (49%) MLCT $\pi_{anc}\rightarrow\pi^*_{anc}$ (33%) LC
S_5	3.42(362)	0.066	$d_{xz}\rightarrow\pi^*_{anc}$ (64%) MLCT	S_{31}	4.69(264)	0.036	$d_{yz}\rightarrow\pi^*_{cycl}$ (53%) MLCT
S_9	3.77(329)	0.027	$d_{xy}\rightarrow\pi^*_{cycl}$ (68%) MLCT	S_{32}	4.71(263)	0.034	$\pi_{cycl}\rightarrow\pi^*_{cycl}$ (53%) LC
S_{11}	3.98(312)	0.057	$d_{xy}\rightarrow\pi^*_{cycl}$(68%) MLCT	S_{35}	4.78(259)	0.068	$d_{xz}\rightarrow\pi^*_{cycl}$ (40%) MLCT $d_{xy}\rightarrow\pi^*_{cycl}$ (32%) MLCT
S_{17}	4.32(287)	0.077	$d_{xy}\rightarrow\pi^*_{anc}$ (43%) MLCT $\pi_{anc}\rightarrow\pi^*_{anc}$ (37%) LC	S_{41}	4.96(250)	0.146	$d_{xy}\rightarrow\pi^*_{cycl}$ (40%) MLCT $d_{xz}\rightarrow\pi^*_{cycl}$ (39%) MLCT
S_{20}	4.42(281)	0.083	$d_{xy}\rightarrow\pi^*_{anc}$ (41%) MLCT $d_{xz}\rightarrow\pi^*_{anc}$ (34%) MLCT				
			[Ir(**a**)$_2$(acac)]				
S_1	3.47(358)	0.011	$d_{xy}\rightarrow\pi^*_{cycl}$ (66%) MLCT	S_{24}	4.68(265)	0.108	$\pi_{anc}\rightarrow\pi^*_{cycl}$ (62%) LC
S_3	3.56(348)	0.058	$d_{xy}\rightarrow\pi^*_{cycl}$ (67%) MLCT	S_{25}	4.74(261)	0.034	$\pi_{anc}\rightarrow\pi^*_{anc}$ (59%) LC
S_6	3.87(320)	0.040	$d_{xz}\rightarrow\pi^*_{cycl}$ (61%) MLCT	S_{27}	4.80(258)	0.032	$\sigma_{Ir-C/O}\rightarrow\pi^*_{cycl}$ (49%) LC
S_{11}	4.31(288)	0.066	$d_{yz}\rightarrow\pi^*_{cycl}$ (65%) MLCT	S_{34}	4.95(250)	0.041	$\sigma_{Ir-C/O}\rightarrow\pi^*_{anc}$ (37%) LC $\sigma_{Ir-C/O}\rightarrow\pi^*_{cycl}$ (33%) LC
S_{16}	4.50(275)	0.057	$d_{yz}\rightarrow\pi^*_{cycl}$ (47%) MLCT	S_{39}	5.04(246)	0.135	$\pi_{cycl}\rightarrow\pi^*_{cycl}$ (38%) LC $n_O\rightarrow\pi^*_{cycl}$ (30%) LC
S_{18}	4.53(274)	0.061	$d_{xy}\rightarrow\pi^*_{cycl}$ (59%) MLCT	S_{43}	5.13(242)	0.037	$n_O\rightarrow\pi^*_{cycl}$ (36%) LC $n_O\rightarrow\pi^*_{cycl}$ (37%) LC
			[Ir(a)$_2$(pic)]				
S_1	2.97(417)	0.001	$d_{xy}\rightarrow\pi^*_{anc}$(70%) MLCT	S_{30}	4.73(262)	0.029	$\pi_{cycl}\rightarrow\pi^*_{anc}$ (48%) LC
S_3	3.57(347)	0.027	$d_{xy}\rightarrow\pi^*_{cycl}$ (77%) MLCT	S_{32}	4.76(261)	0.047	$d_{xz}\rightarrow\pi^*_{cycl}$ (32%) MLCT $\pi_{cycl}\rightarrow\pi^*_{anc}$ (30%) LC
S_8	3.86(322)	0.063	$d_{xy}\rightarrow\pi^*_{anc}$(44%) MLCT $d_{xz}\rightarrow\pi^*_{anc}$ (39%) MLCT	S_{35}	4.92(252)	0.088	$\pi_{cycl}\rightarrow\pi^*_{cycl}$ (53%) LC
S_{14}	4.27(290)	0.028	$d_{yz}\rightarrow\pi^*_{cycl}$ (38%) MLCT $d_{yz}\rightarrow\pi^*_{cycl}$ (30%) MLCT	S_{37}	4.97(250)	0.038	$\pi_{cycl}\rightarrow\pi^*_{cycl}$ (42%) LC $\pi_{cycl}\rightarrow\pi^*_{cycl}$ (36%) LC
S_{15}	4.30(288)	0.029	$d_{xy}\rightarrow\pi^*_{anc}$ (44%) MLCT	S_{38}	4.97(249)	0.031	$d_{xy}\rightarrow d_{z2}$ (26%) MC $\pi_{cycl}\rightarrow\pi^*_{cycl}$ (24%) LC
S_{23}	4.58(271)	0.049	$d_{xy}\rightarrow\pi^*_{cycl}$ (40%) MLCT	S_{44}	5.14(241)	0.047	$\pi_{cycl}\rightarrow\pi^*_{cycl}$ (38%) LC
S_{27}	4.68(265)	0.041	$d_{xy}\rightarrow\pi^*_{cycl}$ (39%) MLCT				

Table 4. Lowest Singlet−Triplet Theoretical Emission Energies by Means of TD-DFT and Δ-DFT Approaches[a]

	[Ir(**a**)$_2$(bpy)]$^+$	[Ir(**a**)$_2$(acac)]	[Ir(**a**)$_2$(pic)]
	TD-DFT Vertical Singlet−Triplet Excitations; ΔE [eV (nm)] and Assignment		
T_1	2.46 (505) ^{3}MLCT	3.00 (413) ^{3}MLCT	2.94 (422) ^{3}MLCT
T_2	2.96 (419) ^{3}MLCT/^{3}LC	3.11 (399) ^{3}MLCT	3.15 (394) ^{3}MLCT
T_3	3.09 (401) ^{3}LC	3.15 (394) ^{3}MLCT	3.21 (386) ^{3}MLCT
T_4	3.22 (384) ^{3}MLCT	3.30 (376) ^{3}MLCT	3.34 (371) ^{3}MLCT
T_5	3.27 (379) ^{3}MLCT/^{3}LC	3.36 (369) ^{3}MLCT	3.36 (369) ^{3}MLCT
	Theoretical $E_{e\text{-}e}$; ΔE [eV (nm)]		
	436	421	417
	Theoretical AEE; ΔE [eV (nm)]		
	581	476	472

[a] The values are obtained in the presence of solvent.

shown in Table 4, the theoretical values of the adiabatic electronic emission (AEE; 581, 476, and 472 nm) obtained as the energy difference between T_1 and S_0 at the optimized T_1 geometry correlate much better to the experimental spectral PL maxima (560, 435, and 527 nm). Additional information is obtained through the $E_{e\text{-}e}$ energies (i.e., the energy differences between T_1 and S_0 minima on each potential energy surface), which can be approximated to the E_{0-0} experimental values, which can be estimated experimentally as the intersection point between the emission and absorption spectra. The theoretical values of 436, 421, and 417 nm, obtained for [Ir(**a**)$_2$(bpy)]$^+$, [Ir(**a**)$_2$(acac)], and [Ir(**a**)$_2$(pic)], respectively, agree well with the experimental ones (474, 400, and 440 nm, compare Table 1).

Conclusion

A series of heteroleptic iridium(III) complexes coordinating new cyclometalating ligands, prepared via "click" chemistry approaches, were synthesized and characterized. The electro-optical properties were discussed in comparison to their corresponding literature-known 2-phenylpyridine-based counterparts. The experimental data were supported by extensive DFT calculations. The spectroscopic results as well as the theoretical studies reveal an increased possibility of color-tuning through changing the ancillary ligand for the new cyclometalated systems associated with the expected blue-shift of the spectral characteristics. Cyclic voltammetry investigations supported by theoretical calculations indicated the destabilization of the LUMOs to be the main reason for this hypsochromicity.

Experimental Section

Materials and General Experimental Details. The solvents were purchased from Biosolve. All chemicals were of reagent grade, obtained from commercial suppliers, and used as received

unless specified otherwise. The ancillary ligand 2-(1-decyl-1*H*-[1,2,3]-triazol-4-yl)pyridine (trpy) was synthesized according to the literature.[27] Modified literature procedures were used for the synthesis of the heteroleptic complexes $[Ir(ppy)_2(acac)]$,[15] $[Ir(ppy)_2(pic)]$,[16] and $[Ir(ppy)_2(bpy)]$.[56,57] Column chromatography was carried out on standardized aluminum oxide 90 (0.063−0.200 mm) or silica gel 60 (0.040−0.063 mm) purchased from Merck. Column chromatographic separations were monitored using Merck 60 F254 precoated silica gel and aluminum oxide sheets and visualized under UV light at $\lambda_{exc} = 254$ and 365 nm, respectively.

Instrumentation. For the microwave experiments a single mode Initiator 8 microwave from Biotage was used. The electromagnetic field had a frequency of 2.45 GHz. For all experiments a fixed temperature was applied, the prestirring time constituted 10 s, and the stirrer rate was set to 600 rpm. 1D (^{1}H and ^{13}C) and 2D (^{1}H−^{1}H gCOSY) nuclear magnetic resonance spectra were recorded on a Varian Mercury 400 MHz instrument at 298 K in deuterated solvents. Chemical shifts are reported in parts per million (δ in ppm) referenced to TMS; coupling constants are given in hertz (Hz). UV−vis absorption spectra were recorded at sample concentrations of 10^{-5} to 10^{-6} mol·L^{-1} on a Perkin-Elmer Lambda 45 UV/vis spectrometer (1 cm cuvettes). Emission spectra and absolute quantum yields were measured on a Perkin-Elmer LS50B luminescence spectrometer and a module system of the C9920 series from Hamamatsu Photonics, respectively. Samples with a concentration of about 10^{-6} to 10^{-7} mol·L^{-1} were investigated. The absorption maxima at the longest wavelengths were chosen for excitation. Cyclic voltammetry (CV) measurements were conducted with an Autolab PGSTAT30 model potentiostat with a standard three-electrode configuration, using a platinum-disk working electrode, a platinum-rod auxiliary electrode, and a Ag/AgCl reference electrode. The experiments were carried out in CH_2Cl_2 containing tetrabutylammonium hexafluorophosphate salt (0.1 mol·L^{-1}) using a scan rate of 100 mV·s^{-1}. Ferrocene was used as internal standard for the determination of the potentials vs SHE and the corresponding HOMO/(LUMO) levels. Matrix-assisted laser desorption-ionization time-of-flight (MALDI-TOF) mass spectrometry was performed on a Voyager-DE PRO Biospectrometry Workstation (Applied Biosystems) time-of-flight mass spectrometer, using dithranol as matrix. Electrospray ionization (ESI) mass spectrometry was conducted on a Finnigan MAT 95XL. Elemental analyses were carried out on a EuroVector EuroEA3000 elemental analyzer for CHNS-O.

Safety Comment. Sodium azide is a very toxic salt, personal protection precautions had to be taken. As, in particular, low-molar-mass organic azides are potentially explosive, attention had to be taken during their handling. Generally, when the total number of carbon (N_C) plus oxygen (N_O) atoms is less than the total numbers of nitrogen atoms (N_N) by a ratio of 3, the compound is considered to be an explosive hazard. Therefore, the compounds were directly prepared prior to use if possible.

1-Decyl-4-phenyl-1*H*-[1,2,3]triazole (H-a). 1-Bromodecane (662 mg, 2.99 mmol) and sodium azide (295 mg, 4.54 mmol, 1.5 equiv) were reacted in ethanol/water (7:3 ratio, 15 mL) at 125 °C under microwave irradiation for 1 h. Afterward, CuI (56.6 mg, 10 mol%) and sodium L-ascorbate (30.4 mg, 5 mol%) as catalyst system as well as phenylacetylene (496 mg, 4.50 mmol, 1.5 equiv) were added, and the reaction mixture was stirred at room temperature for 18 h. The mixture was poured into water (200 mL), and the precipitate was filtered off. The precipitate was dissolved in CH_2Cl_2 (150 mL) and filtered. After washing with water (3 × 80 mL) and drying over $MgSO_4$, the solution was concentrated under reduced pressure and dropped into *n*-pentane. **H-a** was isolated as colorless needles after storing the solution for 3 days in the freezer (652 mg, 76%). ^{1}H NMR (CD_2Cl_2, 400 MHz): δ 7.84 (d, $^3J_{H,H}$ = 7.2 Hz, 2H, H^2), 7.80 (s, 1H, triazole-*H*), 7.44 (m_c, 2H, H^3), 7.34 (t, $^3J_{H,H}$ = 7.4 Hz, 1H, H^4), 4.39 (t, $^3J_{H,H}$ = 7.2 Hz, 2H, N-CH_2), 1.95 (m_c, 2H, N-CH$_2$-CH_2), 1.37−1.29 (m, 14H, (CH_2)$_7$), 0.89 (t, $^3J_{H,H}$ = 7.0 Hz, 3H, CH_3) ppm. ^{13}C NMR (CD_2Cl_2, 100 MHz): δ 147.3, 131.0, 128.8, 127.9, 125.5, 119.6, 50.4, 31.9, 30.3, 29.5, 29.4, 29.3, 29.0, 26.5, 22.7, 13.9 ppm. MALDI-TOF MS (dithranol): m/z = 286.22 ([M + H]$^+$). Anal. Calcd (%) for $C_{18}H_{27}N_3$ (285.43): C, 75.74; H, 9.83; N, 14.54. Found: C, 75.69; H, 9.83; N, 14.54. UV/vis (CH_2Cl_2): λ_{abs} (ε/L·mol^{-1}·cm^{-1}) = 252 (20 100) nm.

4-Decyl-1-phenyl-1*H*-[1,2,3]triazole (H-b). Bromobenzene (631 mg, 4.02 mmol), *N,N′*-dimethylethylenediamine (51.7 mg, 15 mol%), CuI (76.3 mg, 10 mol%), and sodium L-ascorbate (41.4 mg, 5 mol%) were suspended in an ethanol/water mixture (20 mL, 7:3 ratio). The flask was flushed with argon, and NaN_3 (521 mg, 8.01 mmol, 2.0 equiv) was added, a color change to blue could be observed. The reaction mixture was heated to reflux for 3 h. After cooling to room temperature, 1-dodecyne (781 mg, 4.70 mmol, 1.17 equiv) was dropped into the now slightly yellow mixture. The reaction mixture was stirred for 14 h, and the solid was subsequently filtered off, washed with water (3 × 100 mL), and dried. The crude product was dissolved in dichloromethane (200 mL), and the solution was filtered. The organic solution was washed with water (3 × 80 mL) and dried over $MgSO_4$. After gel filtration (silica, CH_2Cl_2 as eluent), the concentrated CH_2Cl_2 phase was dropped into *n*-pentane to precipitate **H-b** as white solid (769 mg, 67%). ^{1}H NMR (CD_2Cl_2, 400 MHz): δ 7.81 (s, 1H, triazole-*H*), 7.75 (d, $^3J_{H,H}$ = 7.6 Hz, 2H, H^2), 7.54 (m_c, 2H, H^3), 7.44 (m_c, 1H, H^4), 2.78 (t, $^3J_{H,H}$ = 7.8 Hz, 2H, N-CH_2), 1.74 (m_c, 2H, N-CH$_2$-CH_2), 1.46−1.23 (m, 14H, (CH_2)$_7$), 0.90 (t, $^3J_{H,H}$ = 7.2 Hz, 3H, CH_3) ppm. ^{13}C NMR (CD_2Cl_2, 100 MHz): δ 149.1, 137.4, 129.6, 128.2, 120.2, 118.8, 31.9, 29.6, 29.4, 29.3, 25.6, 22.7, 13.9 ppm. MALDI-TOF MS (dithranol): m/z = 286.23 ([M + H]$^+$). Anal. Calcd (%) for $C_{18}H_{27}N_3$ (285.43): C, 75.74; H, 9.83; N, 14.54. Found: C, 75.89; H, 9.64; N, 14.71. UV/vis (CH_2Cl_2): λ_{abs} (ε/L·mol^{-1}·cm^{-1}) = 252 (9300) nm.

Tetrakis(1-decyl-4-phenyl-1*H*-[1,2,3]triazolato-C^2,N^3)-(μ-dichloro)diiridium(III) (A). 1-Decyl-4-phenyl-1*H*-[1,2,3]triazole (**H-a**, 158 mg, 0.56 mmol, 2.0 equiv) and $IrCl_3 \times 3H_2O$ (98 mg, 0.28 mmol) were reacted for 14 h in degassed 2-ethoxyethanol/water (12 mL, 3:1 ratio) under reflux excluding light. After cooling to room temperature, water was added and the yellow suspension was extracted with CH_2Cl_2 (150 mL). The organic phase was washed with water (3 × 50 mL) and dried over $MgSO_4$. The concentrated CH_2Cl_2 phase was dropped into *n*-pentane. This procedure was repeated twice to remove unreacted ligand. After gel filtration (Al_2O_3, $CH_3CN \rightarrow CH_3CN/H_2O$ (8:2 ratio) saturated with KNO_3) the precursor complex **A** was obtained as a bright yellow powder (169 mg, 76%). ESI-MS (CH_2Cl_2/CH_3OH): m/z = 1557.5 ([M − Cl]$^+$). Anal. Calcd (%) for $C_{72}H_{104}Cl_2Ir_2N_{12}$ (1593.02): C, 54.29; H, 6.58; N, 10.55. Found: C, 54.27; H, 6.65; N, 10.78.

Tetrakis(4-decyl-1-phenyl-1*H*-[1,2,3]-triazolato-C'^2,N^2)(μ-dichloro)diiridium(III) (B). $IrCl_3 \times 3H_2O$ (314 mg, 0.89 mmol) and 4-decyl-1-phenyl-1*H*-[1,2,3]triazole (**H-b**, 515 mg, 1.81 mmol, 2.0 equiv) were reacted in 52 mL of solvent as described above. After purification, **B** was obtained as a slightly orange powder (375.5 mg, 53%). MALDI-TOF MS (dithranol): m/z = 1557.7 ([M − Cl]$^+$). Anal. Calcd (%) for $C_{72}H_{104}Cl_2Ir_2N_{12}$ (1593.02): C, 54.29; H, 6.58; N, 10.55. Found: C, 54.18; H, 6.91; N, 10.50.

General Procedure for the Synthesis of Charged Ir^{III} Complexes. A mixture of dichloromethane and methanol (9 mL per 0.05 mmol of precursor, 4:5 ratio) was refluxed for 1 h under argon atmosphere. The precursor complex (1.0 equiv) and

(56) Neve, F.; Crispini, A.; Campagna, S.; Serroni, S. *Inorg. Chem.* **1999**, *38*, 2250–2258.
(57) Marin, V.; Holder, E.; Schubert, U. S. *J. Polym. Sci., Part A: Polym. Chem.* **2004**, *42*, 374–385.

2,2′-bipyridine (bpy, 6.0 equiv) or 2-(1-decyl-1*H*-[1,2,3]-triazol-4-yl)pyridine (trpy, 6.0 equiv), respectively, were added. The reaction mixture was stirred for 14 h under reflux excluding light. After cooling to room temperature NH_4PF_6 (5−9 equiv) was added, and the mixture was stirred for 1 h. The solvents were removed under reduced pressure, and the residue was dissolved in CH_2Cl_2 (15 mL). The solution was washed with water (3 × 8 mL) and dried over $MgSO_4$. The concentrated CH_2Cl_2 solution was added dropwise to diethyl ether, and the precipitating solid was filtered off using a glass filter frit and washed with diethyl ether. This precipitation procedure was repeated two times to obtain the charged Ir^{III} complex. When required, further purification was achieved by column chromatography (Al_2O_3, $CH_2Cl_2 \rightarrow CH_2Cl_2/CH_3OH$ (95:5 ratio)).

Bis(1-decyl-4-phenyl-1*H*-[1,2,3]-triazolato-N^3,C'^2)(2,2′-bipyridine)iridium(III) hexafluorophosphate, ([Ir(a)$_2$(bpy)](PF$_6$). Precursor complex **A** (29 mg, 0.02 mmol) and 2,2′-bipyridine (18.0 mg, 0.12 mmol, 6.0 equiv) were reacted according to the general protocol to yield [Ir(**a**)$_2$(bpy)](PF_6) as a yellow powder (37 mg, 90%). ^{1}H NMR (CD_2Cl_2, 400 MHz): δ 8.36 (d, $^3J_{H,H}$ = 7.6 Hz, 2H, bpy-H^6), 8.20 (d, $^3J_{H,H}$ = 5.2 Hz, 2H, bpy-H^3), 8.06 (m_c, 2H, bpy-H^5), 7.81 (s, 2H, triazole-*H*), 7.49 (d, $^3J_{H,H}$ = 7.6 Hz, 2H, H^6 (a)), 7.40 (m_c, 2H, bpy-H^4), 7.03 (m_c, 2H, H^5 (a)), 6.89 (m_c, 2H, H^4 (a)), 6.26 (d, $^3J_{H,H}$ = 7.6 Hz, 2H, H^3 (a)), 4.26 (m_c, 4H, N−CH_2), 1.85 (m_c, 4H, N-CH$_2$-CH_2), 1.52−1.18 (m, 28H, (CH_2)$_7$), 0.89 (t, $^3J_{H,H}$ = 6.2 Hz, 6H, CH_3) ppm. ^{13}C NMR (CD_2Cl_2, 100 MHz): δ 157.1, 156.6, 151.6, 145.9, 138.5, 135.5, 132.4, 128.5, 127.0, 123.2, 122.7, 122.3, 118.3, 52.1, 31.8, 29.7, 29.4, 29.2, 28.8, 26.2, 22.6, 13.8 ppm. MALDI-TOF MS (dithranol): m/z = 917.46 ([M − PF$_6$]$^+$). Anal. Calcd (%) for $C_{46}H_{60}F_6IrN_8P$ (1062.2): C, 52.01; H, 5.69; N, 10.55. Found: C, 52.25; H, 5.65; N, 10.62. UV/vis (CH_2Cl_2): λ_{abs} (ε/L·mol^{-1}·cm^{-1}) = 441 (760), 330 (8600), 299 (21 000), 240 (61 200) nm. Emission (CH_2Cl_2, λ_{exc} = 470 nm): λ_{max} = 550 nm. Quantum yield (CH_2Cl_2, λ_{exc} = 470 nm): Φ_{PL} = 0.45.

Bis(1-decyl-4-phenyl-1*H*-[1,2,3]triazolato-N^3,C^2) (2-(1-decyl-1*H*-[1,2,3]triazol-4-yl)pyridine-N^3,*N*)iridium(III) Hexafluorophosphate, [Ir(a)$_2$(trpy)](PF$_6$). Precursor complex **A** (20 mg, 0.01 mmol) and 2-(1-decyl-1*H*-[1,2,3]triazol-4-yl)pyridine (trpy, 20 mg, 0.07 mmol, 7.0 equiv) were reacted according to the general protocol to yield [Ir(**a**)$_2$(trpy)](PF_6) as a slightly yellow powder after precipitation into *n*-pentane (17 mg, 50%). ^{1}H NMR (CD_2Cl_2, 400 MHz): δ 8.60 (s, 1H, triazole-*H* (trpy)), 8.10 (m_c, 1H, H^6 (trpy)), 8.02−8.00 (m, 1H, H^3, (trpy)), 7.96 (m_c, 1H, H^5 (trpy)), 7.78 (2 × s, 2H, triazole-*H* (a)), 7.45 (m_c, 2H, H^6 (a)), 7.23 (m_c, 1H, H^4, (trpy)), 7.04−6.95 (m, 2H, H^5 (a)), 6.85 (m_c, 2H, H^4 (a)), 6.27−6.22 (m, 2H, H^3 (a)), 4.51 (m, 2H, N-CH_2 (trpy)), 4.36−4.23 (m, 4H, N-CH_2 (a)), 1.99−1.87 (m, 6H, N-CH$_2$-CH_2), 1.48−1.23 (m, 42H, (CH_2)$_7$), 0.90 (m_c, 9H, CH_3) ppm. MALDI-TOF MS (dithranol): m/z = 1047.89 ([M − PF$_6$]$^+$). Anal. Calcd (%) for $C_{53}H_{78}F_6IrN_{10}P$ (1192.43): C, 53.38; H, 6.59; N, 11.75. Found: C, 53.54; H, 6.88; N, 11.90. UV/vis (CH_2Cl_2): λ_{abs} (ε/L·mol^{-1}·cm^{-1}) = 378 (830), 329 (7400), 240 (55 300) nm. Emission (CH_2Cl_2, λ_{exc} = 378 nm): λ_{max} = 495 nm. Quantum yield (CH_2Cl_2, λ_{exc} = 378 nm): Φ_{PL} = 0.29.

Bis(2-phenylpyridinato-*N*,C^2)(2-(1-decyl-1*H*-[1,2,3]-triazole-4-yl)pyridine-N^3,*N*) iridium(III) hexafluorophosphate, [Ir(ppy)$_2$-(trpy)](PF$_6$). Precursor complex **C** (56 mg, 0.05 mmol) and trpy (30 mg, 0.105 mmol, 2.1 equiv) were reacted according to the general protocol to yield [Ir(ppy)$_2$(trpy)](PF_6) as a yellow powder after additional washing with *n*-pentane (85 mg, 90%). ^{1}H NMR (CD_2Cl_2, 400 MHz): δ 8.76 (s, 1 H, triazole-*H*), 8.23 (d, $^3J_{H,H}$ = 7.9 Hz, 1H, trpy-H^3), 8.04 (m, trpy-H^4), 7.96 (d, $^3J_{H,H}$ = 8.2 Hz, 2H, py-H^3), 7.85 (m_c, 1H, trpy-H^6), 7.77−7.83 (m, 2H, py-H^4), 7.74 (m_c, 1H, ph-H^3), 7.70 (m_c, 2H, py-H^6, ph-H^3), 7.52 (d, $^3J_{H,H}$ = 5.1 Hz, 1H, py-H^6), 7.31 (m_c, 1H, trpy-H^5), 7.00−7.10 (m, 4H, 2 × py-H^5 and ph-H^4), 6.94 (m_c, 1 H, ph-H^5), 6.88 (m_c, 1 H, ph-H^5), 6.32 (m_c, 2H, ph-H^6), 4.46 (t, $^3J_{H,H}$ = 6.8 Hz, 2H, N−CH_2), 1.93 (m_c, 2H, N-CH$_2$-CH_2), 1.16−1.37 (m, 14H, (CH_2)$_7$), 0.89 (t, $^3J_{H,H}$ = 6.8 Hz, 3H, CH_3). ^{13}C NMR (CD_2Cl_2, 100 MHz): δ 168.0, 167.4, 150.3, 149.5, 149.3, 148.5, 148.5, 144.0, 139.6, 138.1, 138.0, 131.9, 131.6, 130.5, 129.8, 126.4, 125.7, 124.8, 124.3, 123.3, 123.0, 122.7, 122.2, 119.6, 119.5, 52.5, 31.8, 29.8, 29.4, 29.4, 29.2, 28.8, 26.2, 22.6, 13.9 ppm. Anal. Calcd (%) for $C_{39}H_{42}F_6IrN_6P$ (931.97): C, 50.26; H, 4.54; N, 9.02. Found: C, 50.26; H, 4.48; N, 8.88. UV/vis (CH_2Cl_2): λ_{abs} (ε/L·mol^{-1}·cm^{-1}) = 412 (4400), 384 (5850), 254 (50 500). Emission (CH_2Cl_2, λ_{exc} = 408 nm): λ_{max} = 477 nm. Quantum yield (CH_2Cl_2, λ_{exc} = 408 nm): Φ_{PL} = 0.21.

Bis(1-decyl-4-phenyl-1*H*-[1,2,3]triazolato-N^3,C^2)acetylacetonatoiridium(III), [Ir(a)$_2$(acac)]. The precursor complex **A** (60 mg, 0.04 mmol) was dissolved in degassed ethanol (10 mL), and acetylacetone (Hacac, 40 mg, 0.4 mmol, 10.0 equiv) and sodium carbonate (42.4 mg, 0.4 mmol, 10.0 equiv) were added. The reaction mixture was stirred for 14 h under reflux and exclusion of light. The crude product was purified by column chromatography (Al_2O_3, CH_2Cl_2) to yield [Ir(**a**)$_2$(acac)] as slightly yellow powder (61 mg, 88%). ^{1}H NMR (CD_2Cl_2, 400 MHz): δ 7.76 (s, 2H, triazole-*H*), 7.33 (d, $^3J_{H,H}$ = 7.4 Hz, 2H, H^3), 6.81 (m_c, 2H, H^4), 6.65 (m_c, 2H, H^5), 6.17 (d, $^3J_{H,H}$ = 7.6 Hz, 2H, H^6), 5.21 (s, 1H, acac-C*H*), 4.56−4.44 (m, 4H, N-CH_2), 2.06−2.00 (m, 4H, N-CH$_2$-CH_2), 1.78 (s, 6H, acac-CH_3), 1.41−1.32 (m, 28H, (CH_2)$_7$), 0.91 (t, $^3J_{H,H}$ = 6.8 Hz, 6H, CH_3) ppm. ^{13}C NMR (CD_2Cl_2, 100 MHz): δ 184.8, 157.3, 142.1, 137.0, 134.0, 126.7, 121.1, 120.9, 117.4, 99.8, 52.1, 31.9, 30.1, 29.5, 29.5, 29.3, 29.0, 27.8, 26.3, 22.7, 13.9 ppm. Anal. Calcd (%) for $C_{41}H_{59}F_6IrN_6O_2P$ (860.16): C, 57.25; H, 6.91; N, 9.77. Found: C, 57.60; H, 7.12; N, 9.38. MALDI-TOF MS (dithranol): m/z = 860.65 ([M]$^+$), 761.62 ([M − acac]$^+$).UV/vis (CH_2Cl_2): λ_{abs} (ε/L·mol^{-1}·cm^{-1}) = 312 (9000), 276 (17 000), 241 (41 900) nm. Emission (CH_2Cl_2, λ_{exc} = 318 nm): λ_{max} = 435 nm. Quantum yield (CH_2Cl_2, λ_{exc} = 318 nm): Φ_{PL} = 0.02.

Bis(4-decyl-1-phenyl-1*H*-[1,2,3]triazolato-N^2,C^2)acetylacetonatoiridium(III), [Ir(b)$_2$(acac)]. The precursor complex **B** (59 mg, 0.04 mmol) was dissolved in ethanol (12 mL) and degassed for 1 h under argon. Afterwards, Hacac (100 mg, 1.0 mmol, 25 equiv) and Na_2CO_3 (42 mg, 0.4 mmol, 10 equiv) were added. The reaction mixture was refluxed for 2 days. After cooling to room temperature the solvent was evaporated. The solid was dissolved in CH_2Cl_2 (40 mL), washed with water (3 × 20 mL), and dried over $MgSO_4$. The concentrated solution was dropped into *n*-pentane for precipitation. The crude product was purified further via column chromatography (Al_2O_3, CH_2Cl_2) to yield [Ir(**b**)$_2$(acac)] as a light yellow powder (3 mg, 5%). ^{1}H NMR (CD_2Cl_2, 400 MHz): δ 8.03 (s, 2H, triazole-*H*), 7.28 (d, $^3J_{H,H}$ = 8.0 Hz, 2H, H^6), 6.96 (m_c, 2H, H^5), 6.76 (m_c, 2H, H^4), 6.74 (d, $^3J_{H,H}$ = 7.4 Hz, 2H, H^3), 5.31 (s, 1H, acac-C*H*), 2.91 (t, $^3J_{H,H}$ = 7.4 Hz, 4H, N−CH_2), 1.99 (m_c, 4H, N-CH$_2$-CH_2), 1.83 (s, 6H, acac-CH_3), 1.32−1.28 (m, 28H, (CH_2)$_7$), 0.90 (t, $^3J_{H,H}$ = 7.0 Hz, 6H, CH_3) ppm. MALDI-TOF MS (dithranol): m/z = 861.69 ([M + H]$^+$), 761.63 ([M − acac]$^+$).

Bis(1-decyl-4-phenyl-1*H*-[1,2,3]triazolato-N^3,C^2)(picolinato-*N*,*O*)iridium(III), [Ir(a)$_2$(pic)]. A solution of precursor complex **A** (24 mg, 0.015 mmol) in CH_2Cl_2 (10 mL) was degassed for 1 h. Afterwards, picolinic acid (Hpic, 10 mg, 0.08 mmol, 5.3 equiv) and sodium carbonate (8 mg, 0.08 mmol, 5.3 equiv) were added, and the mixture was refluxed for 14 h. After cooling to room temperature, the organic phase was washed with water (3 × 5 mL) and dried over $MgSO_4$. After column chromatography (Al_2O_3, CH_2Cl_2/CH_3OH (98:2 ratio) as eluent), [Ir(a)$_2$(pic)] was yielded as a yellow powder (13 mg, 47%). ^{1}H NMR (CD_2Cl_2, 400 MHz): δ 8.17 (d, $^3J_{H,H}$ = 7.6 Hz, 1H, pic-*H*), 7.88−7.82 (m, 2H, pic-*H*), 7.78, 7.77 (2 × s, 2H, triazole-*H*), 7.40 (m_c, 2H, H^6), 7.26 (m_c, 1H, pic-*H*), 6.88 (m_c, 2H, H^5), 6.74 (m_c, 2H, H^4), 6.28, 6.20 (2 × d, $^3J_{H,H}$ = 8.8 Hz, $^3J_{H,H}$ = 9.2 Hz, 2H, H^3), 4.45, 4.26 (2 × m_c, 4H, N-CH_2), 1.98, 1.89 (2 × m_c, 4H, N-CH$_2$-CH_2), 1.33−1.28 (m, 28H, (CH_2)$_7$), 0.90 (t, $^3J_{H,H}$ = 6.8 Hz, 6H, CH_3) ppm. ^{13}C NMR (CD_2Cl_2, 100 MHz): δ 172.8, 157.6, 156.8,

153.1, 149.0, 145.1, 142.6, 137.0, 136.4, 136.1, 133.4, 133.1, 127.6, 127.3, 126.9, 126.6, 121.7, 121.5, 121.1, 117.7, 117.5, 52.3, 51.8, 31.8, 30.0, 29.9, 29.4, 29.2, 29.2, 29.0, 28.9, 26.3, 22.7, 13.8 ppm. MALDI-TOF MS (dithranol): $m/z = 844.25$ ($[M + H]^+$), 761.40 ($[M - pic]^+$). Anal. Calcd (%) for $C_{42}H_{56}IrN_7O_2$ (883.41): C, 57.12; H, 6.39; N, 11.10. Found: C, 56.90; H, 6.56; N, 10.80. UV/vis (CH_2Cl_2): λ_{abs} (ε/L·mol^{-1}·cm^{-1}) = 399 (660), 347 (4800), 303 (8900), 243 (43 000) nm. Emission (CH_2Cl_2, λ_{exc} = 399 nm): λ_{max} = 527 nm. Quantum yield (CH_2Cl_2, λ_{exc} = 399 nm): $\Phi_{PL} = 0.11$.

Computational Details. The geometries of $[Ir(\mathbf{a})_2(bpy)]^+$, $[Ir(\mathbf{a})_2(acac)]$, and $[Ir(\mathbf{a})_2(pic)]$ (see Figure 4 for schematic representations) in the electronic singlet ground state and in the lowest triplet excited state were optimized using density functional theory (DFT), as implemented in Gaussian03.[58] The C_{10}-alkyl chain of the 4-phenyl-1*H*-[1,2,3]triazole cyclometalating ligand was replaced by a methyl group for computational ease. The geometries were fully optimized without any symmetry constraints. The hybrid functional B3LYP[59,60] has been combined with a polarized valence triple-ζ basis set (TZVP) for all atoms. Relativistic effects for the iridium atom have been considered using the ECP-60-mwb Stuttgart/Dresden pseudopotential.[61]

Table 5. Main Geometrical Parameters of the Gas Phase Optimized Complexes $[Ir(\mathbf{a})_2(bpy)]^+$, $[Ir(\mathbf{a})_2(acac)]$, and $[Ir(\mathbf{a})_2(pic)]$ in the Ground (S_0) and Lowest Triplet State (T_1)[a]

	$[Ir(a)_2(bpy)]^+$		$[Ir(a)_2(acac)]$		$[Ir(a)_2(pic)]$	
	S_0	T_1	S_0	T_1	S_0	T_1
d_{1-2} [Å]	2.056	2.059	2.050	2.060	2.047	2.047
d_{1-3} [Å]	2.057	2.059	2.050	2.042	2.051	2.056
d_{1-4} [Å]	2.057	2.034	2.038	2.038	2.045	2.043
d_{1-5} [Å]	2.058	2.034	2.038	1.995	2.051	2.001
d_{1-6} [Å]	2.197	2.175	2.186	2.194	2.196	2.228
d_{1-7} [Å]	2.198	2.175	2.186	2.193	2.178	2.175
α_{3-1-2} [°]	171.6	175.3	174.7	175.4	173.9	174.9

[a] The corresponding chemical structures with the atom labeling can be found in Figure 4.

The most relevant calculated geometrical parameters for the complexes $[Ir(\mathbf{a})_2(bpy)]^+$, $[Ir(\mathbf{a})_2(acac)]$, and $[Ir(\mathbf{a})_2(pic)]$ in the electronic singlet ground state (S_0) and in the lowest triplet excited state (T_1) are summarized in Table 5. In general, the bond lengths and angles fit well with those reported experimentally and theoretically for other related heteroleptic Ir^{III} complexes.[62,63] No significant differences have been found among the three complexes, in which the Ir−C^N bond distances (2.04 to 2.06 Å) and Ir−L^X bond distances (around 2.18−2.19 Å) are concerned. A slight variation is found in the different angles between the coordinated nitrogen atoms of the cyclometalating ligand and the Ir^{III} center (α_{3-1-2}), which is close to 175° in the case of $[Ir(\mathbf{a})_2(acac)]$ in comparison to 174° for $Ir(\mathbf{a})_2(pic)]$ and 172° for $[Ir(\mathbf{a})_2(bpy)]^+$, respectively. Regarding the triplet optimized geometries, a shortening of some of the Ir−C^N bond distances with respect to the ground state is found, in particular in the d_{1-5} distance. The angle α_{3-1-2} is larger in all the triplet optimized geometries in comparison to that of the S_0 geometries.

The vertical transition energies have been obtained using TD-DFT[64] at the S_0 optimized geometries. In order to reproduce the measured absorption UV−vis spectra, the first 45 singlet excitations were calculated, with the same functional and basis set as in the optimizations. Since the experimental UV−vis spectra were recorded in solution using CH_2Cl_2 as solvent, the polarization continuum model (PCM; CH_2Cl_2: $\varepsilon = 8.93$) was used. For simulating the phosphorescence emission spectra two types of calculation were performed: (i) TD-DFT singlet−triplet calculations, performed at the ground-state geometry, which provide the vertical absorption energies. Here, the first five vertical low-lying triplet states were obtained, also in the presence of CH_2Cl_2. (ii) Δ-DFT calculations yielding the energy difference between the first triplet excited state at its optimized geometry and the closed-shell ground state at the same geometry in the gas phase, i.e., the adiabatic electronic emission (AEE). This is a simple and reliable way to determine emission energies. Additionally, the theoretical $E_{e\text{-}e}$, which is the energy difference between T_1 and S_0 minima on their corresponding potential energy surface, has been calculated. It is expected that $E_{e\text{-}e}$ energies are close to the E_{0-0} values, i.e., the energy difference between the ground vibrational state of S_0 and T_1, assuming that the zero-point energy of both states does not greatly differ. More accurate energetic values of AEE and $E_{e\text{-}e}$ were obtained through single-point calculations in the presence of solvent (CH_2Cl_2, $\varepsilon = 8.93$) using the PCM algorithm[65,66] as implemented in Gaussian-03 software.

Acknowledgment. The authors acknowledge financial support from the Dutch Polymer Institute (C.U., C.F., A. W.), the Nederlandse Organisatie voor Wetenschappelijk Onderzoek (VICI award for U.S.S.), the Fonds der Chemischen Industrie, and the Carl-Zeiss Stiftung (D.E.). We also thank Rebecca Eckardt (elemental analysis), as well as Tina Erdmenger and Nicole Herzer (MALDI-TOF MS), for help with the respective measurements, and Martin Richter and Jörg Hildebrand for preliminary theoretical calculations. We are grateful to Prof. Dr. Rene Jansen (Eindhoven University of Technology, The Netherlands) for granting access to the analytical setups.

(58) Frisch, M. J.; Trucks, G. W.; Schlegel, H. B.; Scuseria, G. E.; Robb, M. A.; Cheeseman, J. R.; Montgomery, J. A., Jr.; Vreven, T.; Kudin, K. N.; Burant, J. C.; Millam, J. M.; Iyengar, S. S.; Tomasi, J.; Barone, V.; Mennucci, B.; Cossi, M.; Scalmani, G.; Rega, N.; Petersson, G. A.; Nakatsuji, H.; Hada, M.; Ehara, M.; Toyota, K.; Fukuda, R.; Hasegawa, J.; Ishida, M.; Nakajima, T.; Honda, Y.; Kitao, O.; Nakai, H.; Klene, M.; Li, X.; Knox, J. E.; Hratchian, H. P.; Cross, J. B.; Bakken, V.; Adamo, C.; Jaramillo, J.; Gomperts, R.; Stratmann, R. E.; Yazyev, O.; Austin, A. J.; Cammi, R.; Pomelli, C.; Ochterski, J. W.; Ayala, P. Y.; Morokuma, K.; Voth, G. A.; Salvador, P.; Dannenberg, J. J.; Zakrzewski, V. G.; Dapprich, S.; Daniels, A. D.; Strain, M. C.; Farkas, O.; Malick, D. K.; Rabuck, A. D.; Raghavachari, K.; Foresman, J. B.; Ortiz, J. V.; Cui, Q.; Baboul, A. G.; Clifford, S.; Cioslowski, J.; Stefanov, B. B.; Liu, G.; Liashenko, A.; Piskorz, P.; Komaromi, I.; Martin, R. L.; Fox, D. J.; Keith, T.; Al-Laham, M. A.; Peng, C. Y.; Nanayakkara, A.; Challacombe, M.; Gill, P. M. W.; Johnson, B.; Chen, W.; Wong, M. W.; Gonzalez, C.; Pople, J. A.; *Gaussian-03, Revision C.02*.; Gaussian, Inc., Wallingford, CT, 2004.

(59) Becke, A. D. *J. Chem. Phys.* **1993**, *98*, 5648–5652.

(60) Lee, C. T.; Yang, W. T.; Parr, R. G. *Phys. Rev. B* **1988**, *37*, 785–789.

(61) Andrae, D.; Häusermann, U.; Dolg, M.; Stoll, H.; Preuss, H. *Theor. Chim. Acta* **1990**, *77*, 123–141.

(62) Lamansky, S.; Djurovich, P.; Murphy, D.; Abdel-Razzaq, F.; Kwong, R.; Tsyba, I.; Bortz, M.; Mui, B.; Bau, R.; Thompson, M. E. *Inorg. Chem.* **2001**, *40*, 1704–1711.

(63) Cheng-Hsien, Y.; Wei-Lin, S.; Kai-Hung, F.; Shao-Pin, W.; I-Wen, S. *Organometallics* **2006**, *25*, 4514–4519.

(64) Casida, M. E. Time-Dependent Density Functional Response Theory for Molecules. In *Recent Advances in Density Functional Methods*; Chong, D. P., Ed.; World Scientific Publishing Company: Singapore 1995; Part I, pp 155−192.

(65) Cossi, M.; Barone, V.; Mennucci, B.; Tomasi, J. *Chem. Phys. Lett.* **1998**, *286*, 253–260.

(66) Mennucci, B.; Tomasi, J. *J. Chem. Phys.* **1997**, *106*, 5151–5158.